MODELLING OF THE KERF FORMATION THROUGH PRIMARY AND

SECONDARY JET ENERGY FOR THE ABRASIVE WATERJET

E. Uhlmann, C. Männel
Technische Universität Berlin
Berlin, Germany

ABSTRACT

Abrasive waterjet (AWJ) near-net-shape fabrication including AWJ-Milling is a promising non-conventional manufacturing method with advantages for cutting difficult to machine materials. As for AWJ cutting, it is necessary to consider the ratio between the manufacturing time and the workpiece's quality before applying these methods. This ratio is strongly influenced by the AWJ's jet deflection, depending on the AWJ's energy. In this paper a model allowing to predict the kerf formation based on AWJ energy is presented. To study the effects of the AWJ's jet deflection, the AWJ energy is reproduced by a primary and a secondary jet and thus by a primary and secondary material removal. The model was calibrated on titanium aluminide for straight trajectories. The kerf depth and kerf distribution were measured and calculated for curved trajectories. The results reveal that the model reproduces the effects of the kerf formation appropriately. In addition, the model allows to derive strategies to adapt the process and increase the effectiveness of AWJ near-net-shape fabrication.

1. INTRODUCTION

Abrasive waterjet (AWJ) machining is a non-conventional manufacturing technology, that is mainly used for cutting. The technology inheres a couple of advantages including low heat insertion, low cutting forces, an almost unlimited range of material and no interaction between the tool and the workpiece [1, 2]. The last two points also qualify the technology for machining high-performance materials, which are often considered difficult to machine. Since cutting through the materials limits the attainable geometrical freedom of the technology, AWJ milling has been introduced and investigated during the last years [3, 4, 5, 6, 7]. From the various AWJ milling approaches, maskless AWJ milling allows to create 3D shapes without additional preparations. However, knowing the waterjet's behavior during the manufacturing is of crucial importance to describe the resulting kerf and surface formation. Therefore, models have been introduced to describe the kerf profile depending on the AWJ's parameters [3, 6, 8, 9, 10, 11].

The purpose of models for AWJ milling is to predict the material removal by the AWJ and to foresee the attainable geometrical accuracy. Thus, the expected manufacturing time for a given accuracy can be derived and the costs can be estimated. The estimation of quality and time is particularly important if a decision on a manufacturing process chain needs to be taken. This paper aims to improve the prediction quality and range of materials for AWJ machining. Thus, this model can help AWJ manufacturing to be considered more often when designing new process chains.

1.1 AWJ milling

Most of the AWJ milling models focus on brittle materials and do not consider the effects of secondary material removal by the jet deflection [3, 6, 11]. A model by Van Hung Bui at al. [9] describes the problem of the secondary jet and suggests adapting the sweep pitch in order to minimize the jet deflection (jet escape). Unfortunately, this approach can only be used when cutting even surfaces. Furthermore, a common feature of the models is, that they describe the kerf profile through a bijective line or surface. Thus, the models are not able to predict undercuts, which can appear during AWJ machining and milling. Therefore, it must be assumed, that the models do not describe all effects of the AWJ for all kinds of material in detail.

The fundamental erosion behavior of accelerated particles interacting with a solid material has been described by Finnie [12] and Bitter [13]. They show that the angle of cut α is of crucial importance when the material removal rate is observed. The findings show that for brittle materials the maximum depth of cut appears for an angle of cut of $\alpha = 90°$. Ductile materials on the other side show the highest material removal rate (MRR) around the angle of cut of $\alpha = 20°$ [13].

1.2 Modelling of the AWJ

In this paper, the approach introduced by Axinte [6] is used as basis for the prediction of the kerf profile (jet footprint) and is therefore described in more detail. Axinte [6] presented a geometrical approach of the waterjet based on the assumption that the waterjet's energy and thus the etching rate E correlates with the local waterjet velocity profile $V_{(r)}$ exiting the focus tube, formula 1. Thus, the etching rate E only depends on the process parameters such as water pressure p and abrasive mass flow rate $\dot{m}_A$. The etching rate E is a material specific value. In this paper the etching rate E is referred to as primary etching rate E_1, formula 1.

$$E_1(r) = C\,(V_1 \times n_1)^q \qquad \text{Formula 1}$$

The profile of primary etching rate $E_1(r)$ equals the dot product of the waterjet velocity V_1 and the normal vector n_1 extended with a constant values C and a power factor q which must be calibrated through tests, figure 1. The profile of the primary etching rate $E_1(r)$ can also be derived from the time derivation of a measured kerf profile Z, formula 2. By combining both formulae and transforming the equation to be dimensionless, a nonlinear partial differential equation, formula 3, can be established.

$$\frac{\partial Z}{\partial t} = Z(x,y,t)\cdot n_1 \cdot e_{1z} = \frac{-E_1(r)}{\sqrt{1 + \left(\frac{\partial Z}{\partial x}\right)^2 + \left(\frac{\partial Z}{\partial y}\right)^2}} \qquad \text{Formula 2}$$

$$\frac{\partial \bar{Z}}{\partial \bar{t}} = \begin{cases} -\dfrac{\varepsilon \bar{E}\left(\sqrt{\bar{x}^2 + \bar{t}^2}\right)}{\sqrt[k]{1 + \left(\frac{\partial \bar{Z}}{\partial \bar{x}}\right)^2 + \left(\frac{\partial \bar{Z}}{\partial \bar{t}}\right)^2}} & \text{for } -\sqrt{1-\bar{z}^2} \leq \bar{t} \leq \sqrt{1-\bar{z}^2} \\[2em] 0 \text{ for } -1 \leq \bar{t} \leq -\sqrt{1-\bar{x}^2} \text{ and } \sqrt{1-\bar{x}^2} \leq \bar{t} \leq 1 \end{cases} \qquad \text{Formula 3}$$

If high feed speeds v_f are investigated, formula 3 can be further simplified. Afterwards, it is possible to integrate the function to formula 4 which can be inverted to formula 5.

$$\bar{Z}_0(\bar{x}) = -2\varepsilon \int_{\hat{x}}^{1} \frac{\bar{r} * \bar{E}(\bar{r})}{\sqrt{\hat{x}^2 + \hat{t}^2}}\, d\bar{r} \qquad \text{Formula 4}$$

$$\bar{E}(\bar{r}) = \frac{1}{\varepsilon\pi}\left[\int_{\bar{r}}^{1} \frac{R(\bar{Z}_0(R) - \bar{Z}_0(\bar{r}))}{(R^2 - \bar{r}^2)^{\frac{3}{2}}}\, dR - \frac{\bar{Z}_0(\bar{r})}{\sqrt{1-\bar{r}^2}}\right] \qquad \text{Formula 5}$$

Given a measured kerf profile $Z_0(x)$ it is now possible to calculate the specific etching rate $E_1(r)$. Knowing the specific etching rate $E_1(r)$, formulae 3 can be solved numerically and allows the prediction of the kerf profile $Z_1(x)$ for any feed speeds v_f. Axinte [6] showed that the approach works well for SiC ceramic as target material for feed speeds between $v_f = 100$ to 1300 mm/min [6].
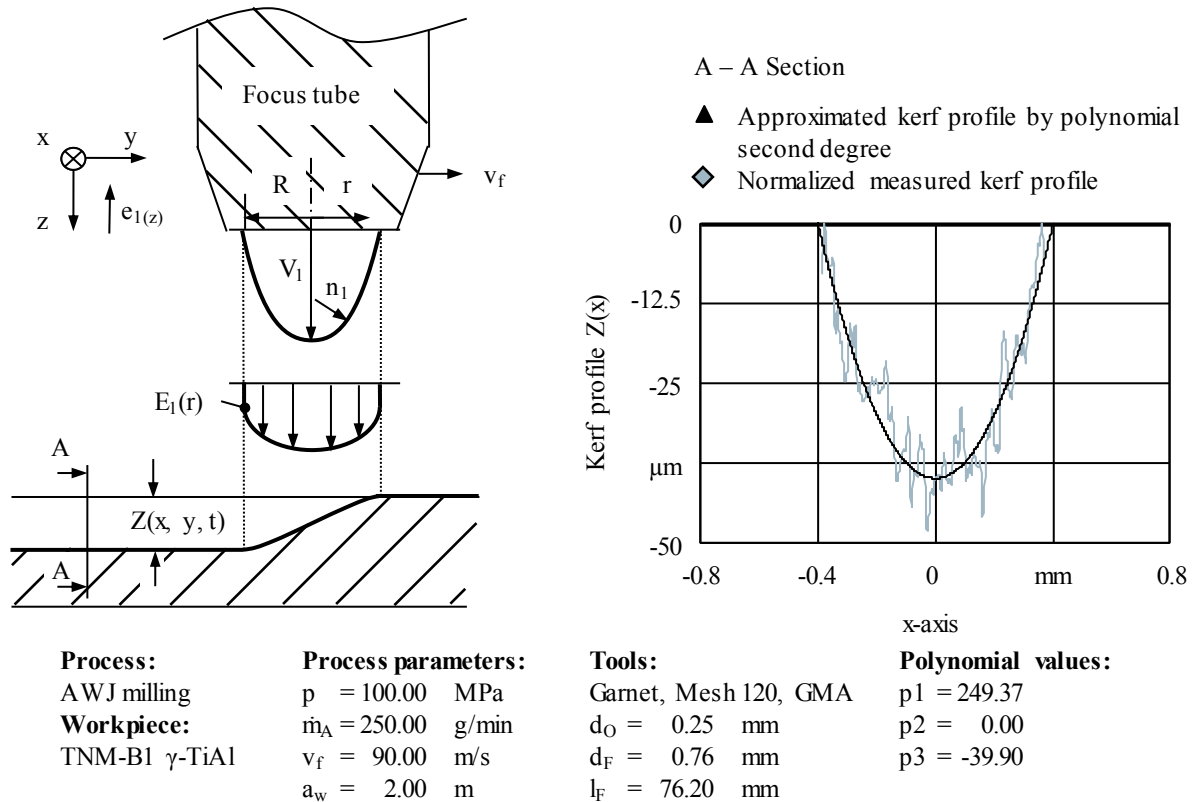

A – A Section

▲ Approximated kerf profile by polynomial second degree

◇ Normalized measured kerf profile

Process:	Process parameters:			Tools:				Polynomial values:	
AWJ milling	p	= 100.00	MPa	Garnet, Mesh 120, GMA				p1 = 249.37	
Workpiece:	$\dot{m}_A$	= 250.00	g/min	d_O	=	0.25	mm	p2 = 0.00	
TNM-B1 γ-TiAl	v_f	= 90.00	m/s	d_F	=	0.76	mm	p3 = -39.90	
	a_w	= 2.00	m	l_F	=	76.20	mm		

Figure 1.   Primary etching rate $E_1(r)$

2. EXPERIMENTAL AND ANALYTICAL INVESTIGATION

The aim of this paper is to expand the analytical approach by Axinte [6] by reducing its boundary conditions, particularly the affinity to brittle material and the trajectory of the abrasive waterjet. First, the trajectory of the waterjet is generalized. Second, the application to mainly brittle target materials is expanded by implementing a secondary jet energy E_2 leading to a secondary material removal Z_2. This extension aims to describe the effects of ductile materials below $v_f = 3600$ mm/min. In the end, a further generalization regarding the angle of cut at $\alpha = 90°$ and flat workpiece will be discussed.

In order to calibrate the model several AWJ milling operations have been performed. The tests were carried out on a waterjet machine of MAXIMATOR JET GMBH, Schweinfurt, Germany, type HRX 160 L using a cutting head with a focus tube length $l_f = 76.2$ mm, a focus diameter

$d_f = 0.76$ mm, an orifice diameter $d_o = 0.25$ mm, a distance between workpiece and focus tube of $l_s = 2$ mm and garnet sand with mesh size 120 of GMA GARNET (EUROPE) GMBH, Hamburg, Germany. The tests and the calculation were implemented for titanium aluminide, type Ti-43,5Al-4Nb-1Mo 0,1B (TNM-B1), of GFE METALLE UND MATERIALIEN GMBH, Nürnberg, Germany.

2.1 Primary Material Removal by the Jet Energy

In order to enable a free movement of the waterjet and variations of the feed speed v_f during a cut, the calculation of the kerfs profile was implemented using MATLAB Release 2015b, the MATHWORKS, INC., Natick, United States. A stepwise algorithm was implemented which assigns a dwell time t_d to every position of the waterjet P_{WJi} along a trajectory. The dwell time depends on the feed speed v_f and the control time t_c. Variations of the control time t_c allow an adjustment towards more precise predictions, or faster calculations. The waterjet positions were extracted from a simple G-Code list allowing the definition of waterjet positions P_{WJ}, feed speeds v_f, radii of the waterjet's trajectory R_{WJ} and the corresponding radii direction (G02, G03), figure 2. Once the waterjet movement and the dwell times t_d were calculated, the effect of the etching rate $E_1(r)$ towards a surface was established. The applied surface consisted of x-, and y-positions between an upper limit UL and a lower limit LL and a defined distance between each point, resolution $res_{i,j}$. All points were defined with a starting z-value of $Z_{1ij} = 0$. The effect of the jet energy was calculated by checking the distance between all points on the surface to the position of the waterjet P_{WJi} for every time step t. If the distance was smaller than the maximum radius of the waterjet $r < R$ the z-value was reduced according to the jets local etching rate $E_1(r)$, formula 6.

$$-\varepsilon_{allg}\bar{E}_1(\bar{r}) = -\frac{v_{f1}}{v_{f2}} \cdot \frac{1}{\pi} \cdot \frac{(p1 - p3 - 2 \cdot p1 \cdot r^2)}{\sqrt{1 - r^2}}$$

Formula 6

The local etching rate $E_1(r)$ has been found according to formula 6. This formula was derived from a measured and simplified kerf profile $Z_0(x)$, for a feed speed of $v_f = 5400$ mm/min, pressure $p = 100$ MPa and an and abrasive mass flow rate of $\dot{m}_A = 250$ g/min. In this paper the kerf profile $Z_0(x)$, formula 7, of a straight trajectory was assumed to be a polynomial second order. Thus, the kerf profile $Z_0(x)$ could be defined by two parameters $p1$ and $p3$. If the profile is symmetric around the x-axis and dimensionless $p1 = -p3$. This approximation allowed a good description of the kerf with a coefficient of determination $R^2 = 0.98$, figure 1.

$$Z_{0(x)} = p1 \cdot x^2 + p3 \ (-1 \leq x \leq 1)$$

Formula 7

Process:
AWJ milling
Tools:
Garnet, Mesh 120, GMA
d_O = 0.25 mm
d_F = 0.76 mm
l_F = 76.20 mm
a_w = 2.00 mm
Workpiece:
TNM-B1 γ-TiAl
Process parameters:
p = 100.00 MPa
$\dot{m}_A$ = 250.00 g/min
v_f = 30.00 m/min

Calculation parameters:
t_c = 0.08 ms
R = 0.40 mm
UL_x = 4.00 mm
LL_x = 0.00 mm
res_x = 0.05 mm
UL_y = 4.00 mm
LL_y = 0.00 mm
res_y = 0.05 mm
$\overline{p1}$ = 39.90 µm
p3 = -39.90 µm

G-Code input file

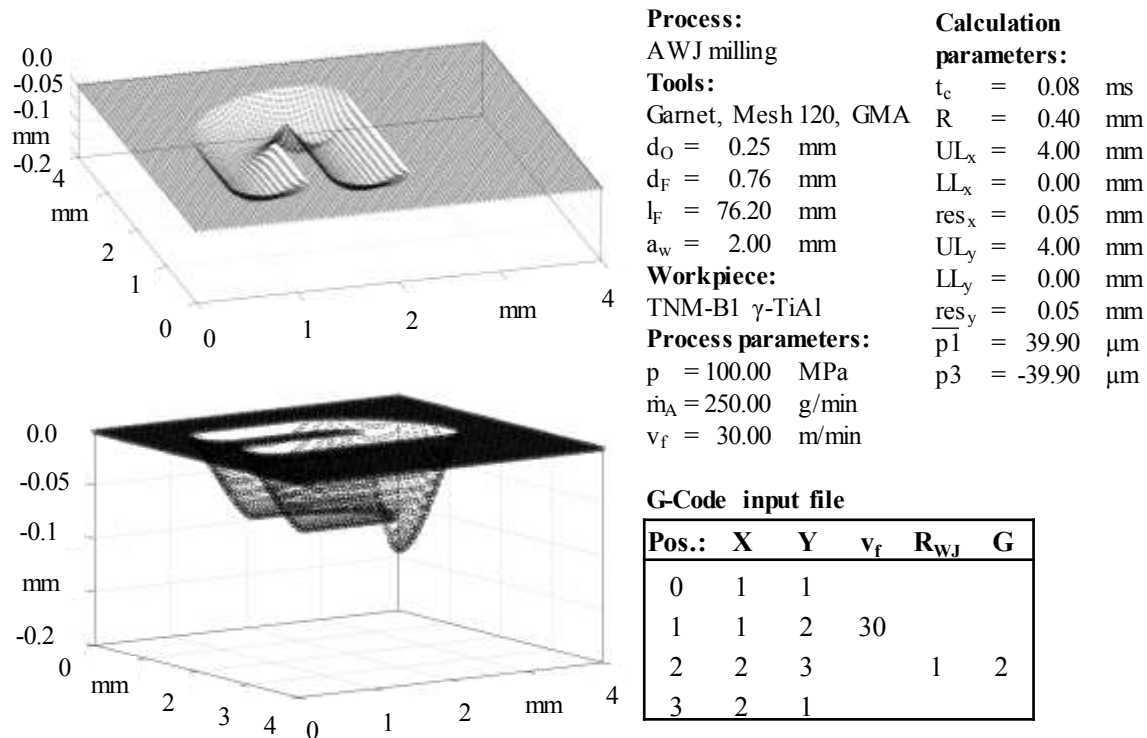| Pos.:	X	Y	v_f	R_{WJ}	G
0	1	1			
1	1	2	30		
2	2	3		1	2
3	2	1			

Figure 2.   Results of the primary etching rate $E_1(r)$ for a free trajectory

Applying the presented approach, the kerf profile can be calculated for any feed speed v_f and waterjet trajectory above a surface. Figure 2 shows the movement of the waterjet along the trajectory given in the G-Code file in the figure. A straight path, a radius and a sharp corner were implemented. It is possible to observe a deeper maximum depth of cut d_c close to the sharp corner. This observation provided prove for the functionality of the approach, since this phenomenon is known, described and discussed by Laurinat [14].

2.2 Secondary Material Removal by the Jet Energy

The approach using a primary jet energy orthogonal to the surface allows a good prediction of the kerf formation, especially for brittle materials and high feed speed v_f [6]. Figure 3 shows that the approach works as well for high feed speeds on the ductile material TiAl TNM-B1. However, below a feed speed of v_f = 3600 mm/min a difference between the calculated $Z_1(x = 0)$ and the measured $Z_0(x = 0)$ kerf profile can be observed.
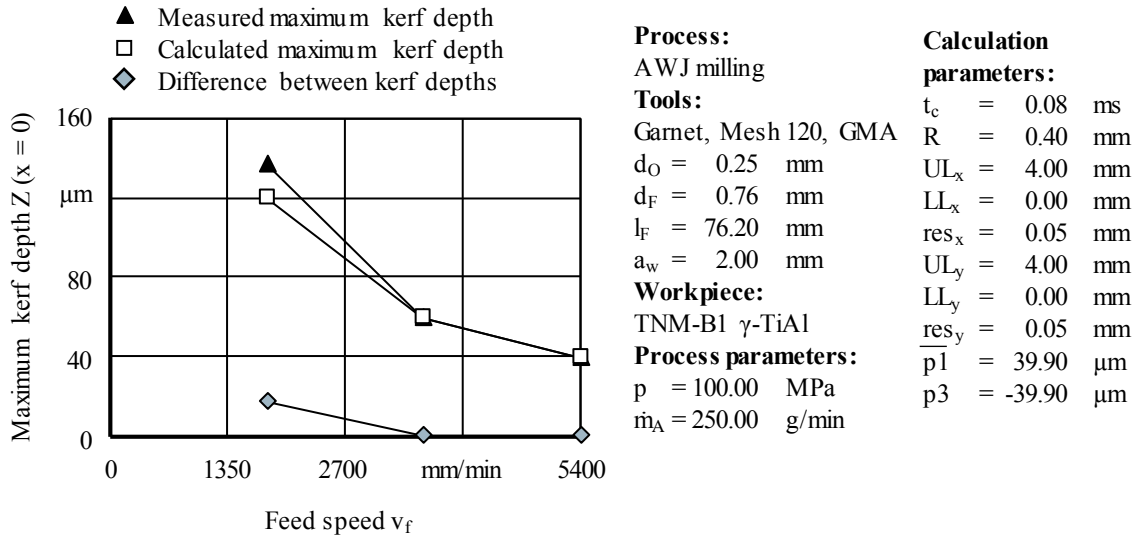
Figure 3. Calibration of the secondary etching rate $E_2(r)$

The additional material removal during low feed speeds v_f is assumed to be a result of the jet deflection or secondary jet. The secondary jet appears if a slant surface is generated during the cutting. This slant surface, around the normal vector n_{WJ} in <u>figure 4</u>, reflects some of the jet's energy, usually against the direction of the feed speed v_f. The reflected secondary jet can cause an additional MRR. The calculation with a primary jet energy works well only for high feed speeds v_f because the dwell time t_d is short, the kerf depth stays low and thus, the surface does not become slant. Consequently, almost no energy is reflected towards other material. The approach using the primary jet energy also works well for brittle materials. This is due to the cutting behavior of the waterjet. Bitter showed [13] that, if the angle of cut α changes from 90° to 70°, the material removal rate MRR of brittle materials decreases only about 8 %. On the other side, the same change in the angle of cut α causes an increase in the MRR of about 50 % for ductile materials. This behavior explains the higher sensitivity of ductile materials towards changes in the feed speed.

In order to establish a prediction method that includes ductile materials and low feed speeds v_f the secondary jet needs to be implemented into the approach. Hence, the direction of the secondary jet e_2 cannot be orthogonal to the workpieces surface. Figure 4 shows the fundamentals for the secondary jet calculation. In this approach it is assumed that the direction of the secondary waterjet points opposite of the surfaces normal vector n_{WJ} in the x-y-plane. In the y-z-plane the direction of the secondary jet e_2 is expected to be orthogonal to the normal vector n_{WJ} and tangential to the slant surface. The strength of the secondary etching rate is defined to close the gap between maximum measured and calculated kerf depth (i.e., figure 3). Thus, the maximum kerf depth of the secondary etching rate creates a kerf profile with $Z_2(x = 0) = 18$ µm for a feed speed of $v_f = 1800$ mm/min.
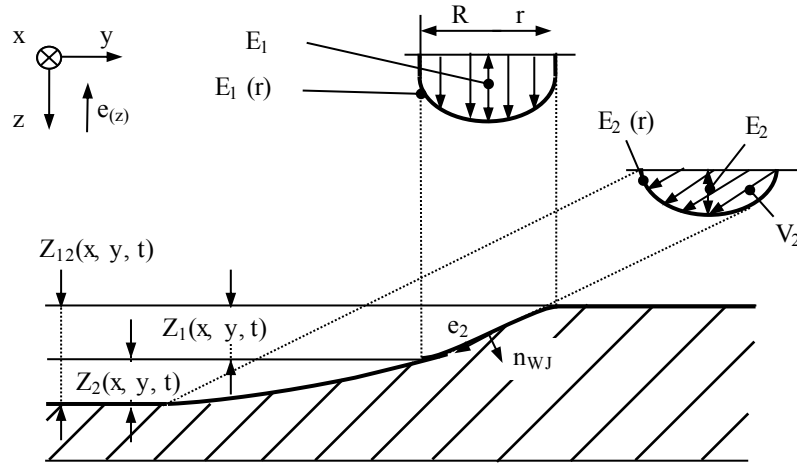
Figure 4. Fundamentals of the primary E1(r) and secondary E2(r) etching rate

In order to implement the secondary material removal Z_2, it was not only necessary to implement the secondary etching rate $E_2(r)$, but also to change the target surface itself. Since the secondary etching rate E_2 adapts the direction according to the surface and undercuts are possible, it is necessary to implement a 3D environment. The 3D environment is realized by adding a dimension for the material in z-direction. Therefore, the z-axis is defined alike the x and y axis with an upper and lower limit (UL_z, LL_z) as well as a resolution res_z. A material element M_{ijk} is added to every point in the 3D matrix. The material element M_{ijk} is defined between 0 to 1. A material element with $M_{ijk} = 1$ states an element that contains full material. The approach allows the reduction of material independent of the direction of an etching rate.

Once the 3D material matrix and the maximum secondary etching rate $E_2(r)$ were defined, an additional calculation step was implemented into the MATLAB program for every time step t after the calculation of the primary material removal. In this step, firstly, the surface normal vector n_{WJ} is calculated. Afterwards, the direction of the secondary jet e_2 is defined, and the secondary etching rate $E_2(r)$ is calculated for every point hit by the waterjet in the x-y-surface. The starting point of the secondary etching rate is the kerf profile created by the primary material removal. From this point the secondary etching rate $E_2(r)$ is directed along the direction of the secondary jet e_2. Every material element M_{ijk} that intersects with the direction of the secondary jet is checked for its value. If the material element value is $M_{ijk} = 0$, the calculations for the secondary jet continuous to the next element $M_{ijk}+e_2$. If the material element value is $M_{ijk} > 0$ the etching rate $E_2(i,j,t)$ reduces the material element M_{ijk} according to the etching rate's value.

Since the defined material element M_{ijk} exist only in a discrete manner, the direction of the secondary jet e_2 had to be limited to these discrete directions as well. Therefore, a matrix was defined to adjust the direction of the secondary jet e_2 to discrete values, with the result, that the direction of the secondary jet e_2 always points at another material element M_{ijk}. This adaption is

dependent on the resolution in x, y and z. The maximum deviation between the direction calculated and the available direction is 6°.
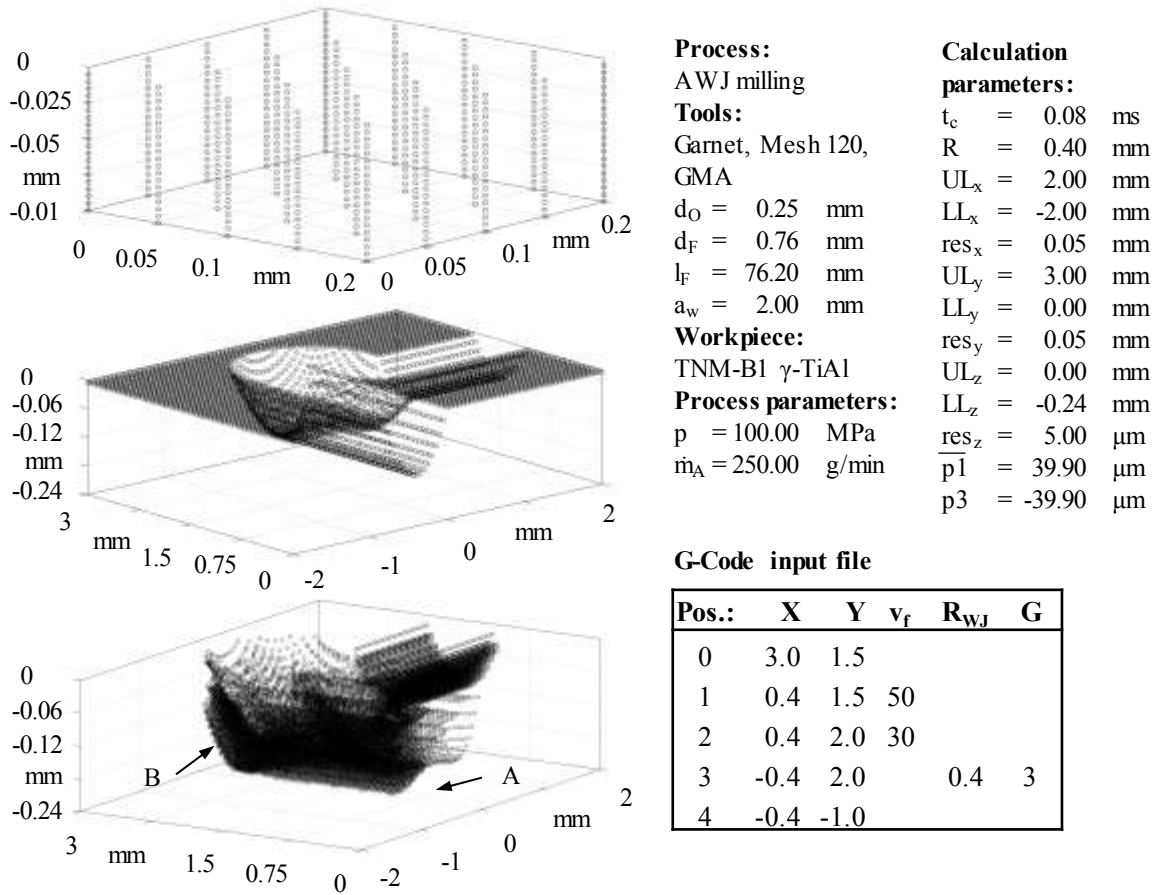

Process:
AWJ milling
Tools:
Garnet, Mesh 120, GMA

d_O =	0.25	mm
d_F =	0.76	mm
l_F =	76.20	mm
a_w =	2.00	mm

Workpiece:
TNM-B1 γ-TiAl
Process parameters:
p = 100.00 MPa
$\dot{m}_A$ = 250.00 g/min

Calculation parameters:

t_c	=	0.08	ms
R	=	0.40	mm
UL_x	=	2.00	mm
LL_x	=	-2.00	mm
res_x	=	0.05	mm
UL_y	=	3.00	mm
LL_y	=	0.00	mm
res_y	=	0.05	mm
UL_z	=	0.00	mm
LL_z	=	-0.24	mm
res_z	=	5.00	µm
$\overline{p1}$	=	39.90	µm
p3	=	-39.90	µm

G-Code input file

Pos.:	X	Y	v_f	R_{WJ}	G
0	3.0	1.5			
1	0.4	1.5	50		
2	0.4	2.0	30		
3	-0.4	2.0		0.4	3
4	-0.4	-1.0			

Figure 5. Results of the simulated primary E1(r) and secondary E2(r) etching rate for a free trajectory

Figure 5 shows the result of the application of the method. The depiction of the secondary jet shows a broad area of material being reached by the secondary jet. In comparison to the primary material removal, the area where the jet exits the workpiece the kerf depth decreases clearly during the last millimeter (A). This behavior is generally known from AWJ cutting [1]. Furthermore, the secondary jet seems to be stronger towards the outer side, during the cutting of a curve (B). To evaluate this effect, a section through a straight part of the trajectory and through the middle of the curve was realized and are shown in figure 6. The relations between the primary $E_1(r)$ and the secondary $E_2(r)$ kerf profile as well as their superposition $Z_{12}(r)$ for a straight trajectory are shown on the left side of the figure. For the straight trajectory the diagram states the relations given in figure 3, where it has been calibrated.

▲ Material removal by primary etching rate $E_1(r)$

☐ Material removal by secondary etching rate $E_2(r)$

◆ Combined material removal (kerf profile) $E_{12}(r)$

– Measured kerf profile $Z_0(r)$

Process:
AWJ milling
Tools:
Garnet, Mesh 120, GMA
d_O = 0.25 mm
d_F = 0.76 mm
l_F = 76.20 mm
a_w = 2.00 mm
Workpiece:
TNM-B1 γ-TiAl

Calculation parameters:
t_c = 0.08 ms
R = 0.40 mm
UL_x = 2.00 mm
LL_x = -2.00 mm
res_x = 0.05 mm
UL_y = 3.00 mm
LL_y = 0.00 mm
res_y = 0.05 mm
UL_z = 0.00 mm
LL_z = -0.24 mm
res_z = 5.00 μm
$\overline{p1}$ = 39.90 μm
p3 = -39.90 μm

Process parameters:
p = 100.00 MPa
$\dot{m}_A$ = 250.00 g/min
G-Code input file

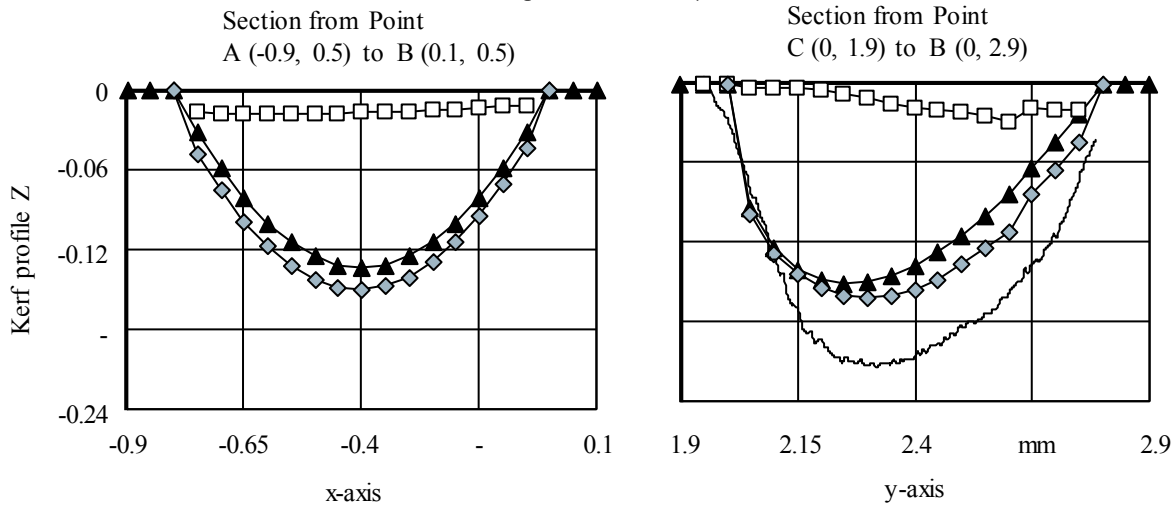| Pos.:	X	Y	v_f	R_{WJ}	G
0	3.0	1.5			
1	0.4	1.5	50		
2	0.4	2.0	30		
3	-0.4	2.0		0.4	3
4	-0.4	-1.0			

Figure 6. Comparison of kerf profiles Z

On the right side of the figure 6 the same profiles are shown for a curve. The diagram shows how the relations and the distribution of the calculated kerf profiles change. First, the peak of primary kerf profile $Z_1(r)$ is displaced from the middle of the jet towards the inner side (left side). The effect of the secondary material removal Z_2 grows stronger towards the outer side of the radius (right side). In combination a calculated kerf profile Z_{12} similar to the one of straight trajectories ensues. The effects of cutting curves have previously been investigated. This investigation states that the overall material removal does not change much from straight trajectories [15]. Thus, the calculated results seem to be in accordance with these findings. The measured kerf profile is about a third deeper than calculated. Hence, a direct validation of the calculation on the measured kerf profile Z_0 is not possible. The difference between the measured and the calculated profile can be explained by the drop in the feed speed v_f due to the inevitable deceleration and acceleration of the manufacturing machine. The problem is described in detail by Klocke [10]. If the differences between the depth of the profiles are left aside, the form of both the analytical and the measured profiles can still be compared. For this comparison, first, the coefficient of determination between the measured kerf profile $Z_0(r)$ and the primary kerf profile $Z_1(r)$ is calculated with R^2 = 76 %. If

the secondary etching rate E_2 is added to the primary profile Z_1 the coefficient of determination becomes $R^2 = 86 \%$. Thus, the test result shows that applying the secondary jet energy improves the quality for the prediction for lower feed speeds v_f on ductile material. The model will be particularly helpful to design the cutting strategies, with minimized errors, for geometries given in figure 7.
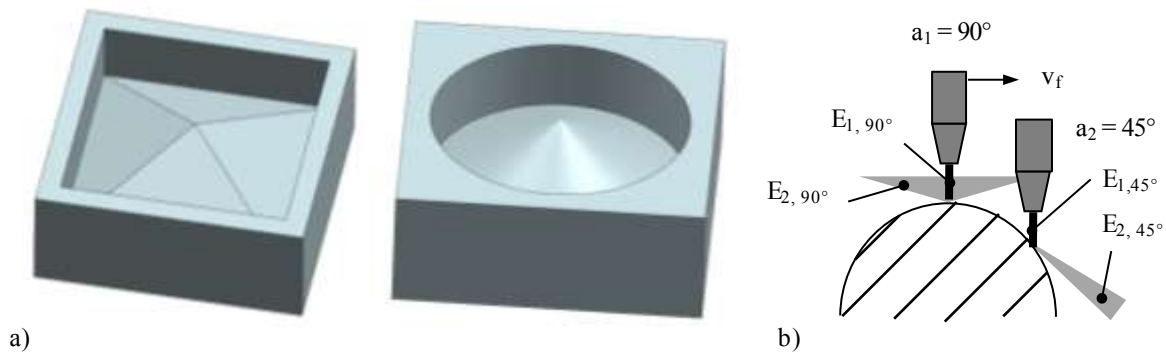

a)   b)

Figure 7.   a) Examples of geometries suitable for modelling with the primary and secondary jet energy; b) Manufacturing of various angle of cuts α

3. CONCLUSION

A model to predict the kerf profile for AWJ milling by implementing a primary and secondary jet energy has been introduced and the capabilities of the approach have been demonstrated. The model is based on the energy of the waterjet as introduced by Axinte [6], broadened by applying a secondary jet and its energy. This extension allows a more accurate prediction of the kerf profiles for lower feed speeds and in particular for ductile materials. Furthermore, the jet movement can be controlled by a G-Code file allowing a wide range of movements. In addition, the target material surface has been set up to enable undercuts in the material. The results show that the calculation can reproduce specific behaviors of the waterjet such as the exiting behavior and the kerf formation cutting radii.

4. OUTLOOK

As described, ductile materials react very sensitively towards changes in the angle of cut α. Therefore, the primary and the secondary jet energy must be calibrated and implemented in the model for different angles of cut $\alpha \neq 90°$ (figure 7). In addition, the calculation results might be further improved by applying a normal vector for each finite element n_{WJij} that is targeted by the waterjet. The result would be a different secondary jet direction for each finite waterjet. Once the comprehensive model has been established, it should be able to, not only predict the kerf profile, but also be used to quickly apply changes in the waterjet parameter settings for specific problems

and analyze the resulting kerf profile $Z(r)$. These findings could be used to derive acceleration and accuracy requirements for new AWJ milling machines.

5. ACKNOWLEDGMENTS

6. REFERENCES

[1]   Hashish M.: A Modeling Study of Metal Cutting with Abrasive Waterjets. Journal of Engineering Materials Technololy 106 (1986), p. 88 - 100.

[2]   Hashish, M.: Wear in Abrasive-Waterjet Cutting Systems. Wear of Materials (1987), p. 769 - 776.

[3]   Zeng, Jiyue; Kim, Thomas J.: An erosion model for abrasive waterjet milling of polycrystalline ceramics. Wear 199 (1996), p. 275 - 282.

[4]   Hashish, M.: Controlled-Depth Milling of Isogrid Structures with AWJs. Journal of Manufacturing Science and Engineering. 120 (1998), p. 21 - 27.

[5]   Fowler, G.; Shipway, P; Pashby, I.: Abrasive water-jet controlled depth milling of Ti6Al4V alloy - an investigation of the role of jet - workpiece traverse speed and abrasive grit size on the characteristics of the milled material. Journal of Materials Processing Technology (Journal of Materials Processing Technology). 161 (2005) p. 407 - 414.

[6]   Axinte DA, Srinivasu DS, Billingham J, Cooper M. Geometrical modelling of abrasive waterjet footprints: A study for 90° jet impact angle. CIRP Annals - Manufacturing Technology 59, 2010, p. 341 - 346.

[7]   Faltin, F.: Endkonturnahe Schruppbearbeitung von Titanaluminid mittels Wasserabrasivstrahlen mit kontrollierter Schnitttiefe. Berichte aus dem Produktionstechnischen Zentrum Berlin. Hrsg.: Uhlmann, E. Dissertation, Technische Universität Berlin. Stuttgart: Fraunhofer IRB, 2018.

[8]   EITobgy, M.; Ng, E-G.; Elbestawi, M. A.: Modelling of Abrasive Waterjet Machining, A New Approach. CIRP Annals - Manufacturing Technology 54, 2005, p. 285 - 288.

[9]   Van Bui H, Gilles P, Sultan T, Cohen G, Rubio W. A new cutting depth model with rapid calibration in abrasive water jet machining of titanium alloy. The International Journal of Advanced Manufacturing Technology 93 (2017), p. 1499 - 1512.

[10]   Klocke F, Schreiner T, Schüler M, Zeis M. Material Removal Simulation for Abrasive Water Jet Milling. Procedia CIRP 68, 2018, p. 541 - 546.

[11]   Kong MC, Anwar S, Billingham J, Axinte DA. Mathematical modelling of abrasive waterjet footprints for arbitrarily moving jets: Part I-single straight paths. International Journal of Machine Tools and Manufacture 53 (2012), p. 58 - 68.

[12]   Finnie, I.: The mechanism of erosion of ductile metals. Proceedings of the 3rd US National Congress of Applied Mechanics, Rhode Island, USA, 1958, p. 572 - 532.

[13]   Bitter, J. G. A.: A study of erosion phenomena - Part II. Wear, Vol. 6, Issue 3, 1963, p. 169 - 190.

[14]   Laurinat, A.: Abtragen mit Wasserabrasivinjektorstrahlen. Dissertation, Universität Hannover, 1994.

[15]   Uhlmann, E.; Männel, C.: Effects of Abrasive Waterjet Trepanning on the Kerf Formation. Proceedings of the 24th BHR: BHR Group, 2018, p. 155 - 165.

7. NOMENCLATURE

Symbol	Unit	Definition
α	°	Angle of cut
AWJ	-	Abrasive waterjet
C	1	Constante
d	mm	Diameter
d_c	mm	Depth of cut
d_d	mm	Orifice diameter
d_f	mm	Focus nozzle diameter
DFG	-	German Research Foundation
E	mm/s	Etching rate
e_2	1	Direction of the secondary jet
G	-	G-Code for the direction of the waterjet
LL	mm	Lower limit
l_f	mm	Focus nozzle length
$\dot{m}_A$	g/min	Abrasive flow rate
n	1	Normal vector
n_{WJ}	1	Surfaces normal vector
n_{WJij}	1	Surfaces normal vector for particular position
p	MPa	Pressure
P_{WJ}	mm	Position of the waterjet
R	mm	Maximum radius of the waterjet
R_{WJ}	mm	Radius of the waterjet's trajectory
r	mm	Radius
res	mm	Resolution
t	S	Time step
t_c	S	Control time
t_d	S	Dwell time
UL	mm	Upper limit
V	m/s	Waterjet velocity
v_f	mm/min	Feed speed
V(r)	m/s	Waterjet velocity profile
q	0	Power factor
Z	mm	Kerf profile
Indices		Definition
0		Measured
1		Primary
2		Secondary
i		X-direction
j		Y-direction
k		Z-direction
$-$		Normalized value